Available online at www.sciencedirect.com
SCIENCE DIRECT
Journal of Catalysis 238 (2006) 67–78
JOURNAL OF CATALYSIS
www.elsevier.com/locate/jcat

Characterization and catalytic study of Pt–Ge/Al_2O_3 catalysts prepared by organometallic grafting

Attila Wootsch [a,*], Zoltán Paál [a], Nóra Győrffy [a], Serge Ello [b], Irina Boghian [b], Julie Leverd [a,b], Laurence Pirault-Roy [b]

[a] *Institute of Isotopes, Hungarian Academy of Sciences, PO Box 77, Budapest, H-1525, Hungary*
[b] *Faculté de Science, LACCO, UMR 6503 CNRS, Université de Poitiers, 40 Av. Recteur Pineau, F-86022 Poitiers cedex, France*

Received 21 September 2005; revised 23 November 2005; accepted 24 November 2005

Available online 9 January 2006

Abstract

Ge was added to 1% Pt/Al_2O_3 catalyst by controlled surface reaction of Ge(n-C_4H_9)$_4$ in amounts corresponding nominally to 1/12, 1/8, 1/2, 1, or 2 monolayers. These Pt–Ge/Al_2O_3 catalysts were characterized by FTIR of CO, TEM, H_2 chemisorption, and EXAFS as well as tested in catalytic reactions, that is, transformation of hexane, benzene and cyclohexene in the presence of excess hydrogen. Loading of Ge in amounts of 1/12–1/2 monolayers resulted in catalysts with "bimetallic surface." Loading of 1/12 monolayer of Ge resulted in randomly deposited Ge atoms on the surface of Pt. It hardly affected the catalytic behavior as compared with the Ge-free parent catalyst; 1/8 monolayer of Ge was still located on Pt as single atoms (as shown by EXAFS), but Ge selectively poisoned high coordination sites, active in benzene hydrogenation. This reaction was completely suppressed here, whereas this catalyst was most active in cyclohexene transformation. Pt with 1/8 and 1/2 monolayers of Ge transformed hexane with high selectivity into saturated C_6 products and formed hardly any benzene. The formation of cyclohexane from hexane was also observed, not typical for monofunctional Pt catalysts. Adding 1–2 monolayers of Ge caused a new type of interaction between Pt and Ge containing sites that adsorbed CO but did not adsorb hydrogen. A solid solution of Pt–Ge may have arisen here, creating "bulk bimetallic catalysts" with somewhat more surface Pt atoms not interacting with Ge. These catalysts behaved similarly in hydrocarbon transformations as the original parent catalyst. The possible reaction mechanism of hexane transformation is discussed in detail, in terms of thermodynamic limitations of benzene formation and possible surface species.

Keywords: Organometallic grafting; Pt–Ge catalyst; Hexane; Benzene; Cyclohexene; EXAFS

1. Introduction

Chemical industry needs more and more catalysts producing the desired products with high selectivity generating less waste. These so-called "tailor-made" catalysts generally require special, novel catalyst preparation processes. A deeper understanding of preparation methods and improved bimetallic catalytic systems are important research areas. The behavior of bimetallic catalysts are obviously different from monometallic catalysts in various reactions [1–4]. The way in which the additive component modifies the properties of the pure metal is not yet fully elucidated, however.

Two main types of controlled surface reaction (CSR) are used to prepare tailor-made bimetallic catalysts: surface redox reactions [2,5–7] and organometallic grafting [3,8–14]. These methods lead to specific metal–metal interactions, and the resulting catalysts appear to be specific in various reactions, such as selective hydrogenation of unsaturated compounds [7,9,15,16] and transformation of hydrocarbons [9,12–14,17,18].

Platinum-based monometallic and bimetallic catalysts are of great interest of naphtha reforming. Commercial reforming commonly involves Pt–Re, Pt–Ir, Pt–Sn, and possibly Pt–Ge catalysts [19]. The addition of a second metal to Pt has a beneficial effect on the catalytic performance [20]. Metals with low dehydrogenation activity, such as Re, Sn, and Ge, hinder the

* Corresponding author. Fax: +36 1 392 2533.
E-mail address: wootsch@iki.kfki.hu (A. Wootsch).

0021-9517/$ – see front matter
doi:10.1016/j.jcat.2005.11.035

formation of unsaturated surface species that can form carbonaceous deposits [1,21–23]. Others, such as Ir and Rh, fragment the coke precursors and thereby hamper deactivation [1,21–23]. The addition of a second metal also impedes deactivation by ensemble effect [1]. The second metal (particularly Sn) prevents the sintering of Pt particles during the refining process [19,24]. Industrial reforming requires further development [25–27] due to strict environmental requirements, such as a decrease in the permitted amount of aromatics in gasoline [28]. The desired aims can be achieved by modifying the catalyst support [29] and/or modifying the metallic particles [14].

In a preliminary study [14], we added germanium by controlled surface reaction to a 1% Pt/alumina catalyst in nominal amounts of 1/8 and 2 monolayers. These samples were tested in transformation of hexane, cyclohexene, and benzene in the presence of excess hydrogen. With addition of 1/8 monolayer of added germanium, the catalyst showed high selectivity to produce saturated C_6 products in hexane transformation [14]. At the same time, it was inactive in benzene hydrogenation but was able to hydrogenate cyclohexene. In contrast, the catalyst containing 2 monolayers of germanium behaved similarly to the Ge-free "parent" sample and gave the highest reaction rates, likely by preventing accumulation of deactivating carbonaceous residues. These latter catalysts were active in both cyclohexene transformation and benzene hydrogenation. It was concluded that adding small amounts of Ge decreased the abundance of triangular three-atom Pt ensembles necessary for the chemisorption of the aromatic ring parallel to the surface [30], thereby hampering both hexane aromatization and benzene hydrogenation [14].

In the present paper we extend our earlier study [14] to a wider range of catalysts, including 1/12–2 monolayers of Ge on Pt/Al_2O_3. The unusual catalytic properties (arising as a consequence of a special preparation technique) are interpreted based on combining detailed catalyst characterizations and appropriate catalytic test reactions.

2. Methods

2.1. Catalysts preparation

The parent (**P**) monometallic Pt/Al_2O_3 catalyst was prepared by ion exchange of $Pt(NH_3)_2(NO_3)_2$ in ammonia solution (pH = 12) on a Degussa δ-alumina (surface area, 100 $m^2\,g^{-1}$; particle size, 0.1–0.25 mm). The Pt content was 1 wt%. After drying overnight at 393 K, the catalyst powder was calcined in flowing air at 773 K for 4 h and then reduced at 773 K for 8 h in pure hydrogen flow. The dispersion was 72–76% as measured by different techniques (Table 1).

Bimetallic Pt–Ge samples were obtained by using the surface organometallic grafting method [2,3,8,9,12–14,31] in an in situ reactor [8,12–14]. The prereduced parent sample (using H_2 flow at 473 K for 2 h, followed by cooling in Ar flow) was immersed in heptane solution in Ar atmosphere. After hydrogen adsorption (293 K for 1 h), the organometallic compound, $Ge(n\text{-}C_4H_9)_4$, was anchored in Ar at 343 K for 6 h. The samples were then washed with heptane and dried in Ar flow at 393 K for 1 h and finally reduced in H_2 flow (473 K for 4 h). The amount of $Ge(n\text{-}C_4H_9)_4$ introduced was selected in such a way as to obtain 1/12, 1/8, 1/2, 1, and 2 monolayers of Ge, as calculated for surface Pt atoms.

2.2. Catalyst characterizations

The metal accessibility was determined by three different techniques: hydrogen chemisorption, electron microscopy, and CO-FTIR measurements. The volumetric hydrogen chemisorption was carried out on prereduced samples (473 K, $p = 75$ kPa, H_2 flow for 1 h) after evacuation at room temperature in an apparatus described previously [12]. Transmission electron microscopy (TEM) was performed with a Philips CM120 electron microscope operating at 120 kV with a theoretical resolution of 0.35 nm. Samples were included in a polymeric resin and cut into small (about 40 nm) sections with a diamond knife. Cuts were put onto a TEM grid. The average particle size (average diameter) was determined on several pictures using the formula $\sum n_i d_i^3 / \sum n_i d_i^2$. The Fourier transformation infrared (FTIR) spectra were collected with a Nicolet Magna-750 spectrometer. The samples (about 40 mg) were pressed into pellets and reduced in situ in the spectrometer at 473 K in H_2 flow for 1 h, followed by outgassing and cooling to ambient temperature. CO chemisorption was performed at room temperature by injecting pulses in the cell until the apparent saturation of the catalysts was reached. The dispersion was determined from the peak area of the linearly adsorbed CO species ($\sim$2060 cm^{-1}) using a predetermined calibration curve [32].

Details of EXAFS experiments and their evaluation have been reported earlier [33]. Briefly, synchrotron radiation from a DCI storage ring of 1.85 GeV with an average current of 250 mA was used at the XAS-IV station at the Laboratoire d'Utilisation du Rayonnement Electromagnétique (LURE) in Orsay, France. The measurements were collected at the L_{III} edge of Pt (11.564 keV) using a Si(111) monochromator. The X-ray energy was typically varied from 150 to 600 eV. Spectra were recorded at room temperature in transmission mode using fine powder of the samples, in the range of 11450–12300 eV to exclude the K edge of germanium (11103 eV) from the analysis. The EXAFS signal was extracted from raw data by a conventional procedure to isolate the contribution of the first coordination sphere of Pt [34]. Phase shifts and backscattering amplitudes were obtained from reference compounds (β-PtO_2, Pt metal) under same conditions. Because no good reference compound was available for Pt–Ge in the L_{III} edge of Pt, theoretical parameters were used considering the $PtGe_2$ system [35].

2.3. Catalytic test

Catalytic tests were carried out in a closed-loop reactor ($\sim$70 ml volume) described previously [36,37]. It was filled with a mixture of 1.3 kPa hydrocarbon—hexane (nH), benzene (B), or cyclohexene ($cH^{=}$)—and hydrogen (8–64 kPa). The hexane conversion was studied in the temperature range of 513–633 K, whereas the transformation of benzene and cyclohexene was studied at 363–473 K. Two lots of all catalysts

were used (ca. 20 mg each), one in hexane reaction, prereduced in situ at 653 K with 53 kPa H_2 for 1 h and the other in benzene and cyclohexene transformation, prereduced in situ at 483 K with 53 kPa H_2 for 1 h. Product analysis was performed by gas chromatography using a 50-m CP-Sil 5CB glass capillary column and a flame ionization detector [36,37]. Turnover frequency (TOF) values [38] were calculated as the number of hexane molecules reacted per surface Pt atom, calculated from either CO or hydrogen adsorption (Table 1), using the length of the run as the "contact time" [37]. Regeneration between the runs was carried out at the reaction temperature with 4 kPa air for 2 min, followed by evacuation and hydrogen treatment for 3 min at 13.3 kPa. Standard test reactions [39–42] of hexane transformation ($p(n\mathrm{H}):p(\mathrm{H_2}) = 1.3{:}16$ kPa; $T = 603$ K) were also carried out after exposing the catalysts to hexane/hydrogen mixture at 603 K, $p(n\mathrm{H}):p(\mathrm{H_2}) = 1.3{:}8.0$ kPa for 20 min without regeneration. Results obtained on these intentionally carbonized samples (TOF and S) were compared with reproducible results [36,41] on regenerated catalysts (TOF_0, S_0).

3. Results

3.1. Characterization

The accessibility of surface Pt atoms was measured by H_2 chemisorption and CO adsorption techniques. Average particle size was calculated based on these measurements considering pure Pt, and compared with data measured by TEM (without distinguishing between Pt and Ge). Different techniques gave coherent results for samples with low Ge loading (Table 1). But the H_2 chemisorption values gave significantly less surface Pt than that measured on IR spectroscopy of CO adsorption for **Ge1** and **Ge2** catalysts (Table 1). Accordingly, the particle size values from H_2 chemisorption (Table 1) were significantly higher, but these may not have much physicochemical meaning in this case. Further, the average particle size estimated from CO adsorption was in fair agreement with those measured by TEM (Table 1).

Because germanium does not adsorb hydrogen or CO, and further TEM and EXAFS results exclude sintering of Pt crystallites, we can assume that the presence of Ge on Pt ensembles induced this special adsorption pattern. The chemisorption of hydrogen occurs after dissociation of the H_2 molecule; therefore, it requires two neighboring active surface sites. In turn, CO (with its lone electron pair) could chemisorb after impinging on a surface. These two catalysts have single Pt atoms surrounded by Ge that can apparently adsorb CO in the linear mode (as confirmed from IR spectra; not shown), whereas fewer active doublets are available for H_2 dissociation.

Typical raw Fourier transform EXAFS plots at the L_{III} edge of platinum obtained for **Ge1/2** is presented in Fig. 1. These plots exhibit two predominant peaks for all samples. The first peak corresponds to Pt–O bond (2.04 Å in the reference) and the second peak corresponds to Pt–Pt or Pt–Ge distances (Fig. 1b). This latter peak was 2.775 Å for the platinum reference and 2.76 Å calculated from FEFF code in agreement with earlier findings [35]. No acceptable fitting accuracy (accuracy factors in the range of $4.2–7.5 \times 10^{-3}$) was obtained when considering only the Pt–O and Pt–Pt contributions to modeling the EXAFS signal. Better accuracy factors within one order of magnitude ($5.9–8.2 \times 10^{-4}$) were, however, achieved by also introducing the Pt–Ge contribution (see Fig. 1a). These results confirmed the presence of Ge in the first coordination sphere of platinum in all samples. Results of EXAFS characterization are summarized in Table 1, including N (coordination number) and R (bond length) values of Pt with its Ge neighbors. Pt and O neighbors are omitted, because all samples exhibited similar behavior:

(i) A relatively low Pt–Pt coordination number (near 5.9) indicates the presence of small clusters in correlation with TEM results.
(ii) The Pt–Pt distance (2.72 Å) was slightly smaller than the theoretical value.
(iii) A high Pt–O contribution ($N = 2.3–3.0$) was in accordance with the storage of the samples in air.
(iv) The Pt–O distance (2.05 Å) was very close to the expected distance (2.04 Å).

The values in Table 1 focus on Pt–Ge distance and the number of Ge in the first coordination sphere of platinum. They suggest that Ge is located mostly on Pt surface in the **Ge1/12**, **Ge1/8**, and **Ge1/2** samples. We call these samples "surface bimetallics." Here Pt had few Ge neighbors and had longer Pt–Ge bonds (Table 1). In contrast, in the **Ge1** and **Ge2** sam-

Table 1
Nominal Ge content, metallic accessibility values of the Pt–Ge/Al_2O_3 catalysts as measured by different techniques, and structural parameters of Ge only neighbors in the Pt environment as determined by EXAFS characterization (Pt and O neighbors are omitted)

Catalysts	Introduced Ge		Accessible Pt (%)		Particle size (nm)			EXAFS	
	Monolayer	ppm	H_2 ads.	CO-IR	TEM	H_2 ads.[a]	CO-IR[a]	Ge [N, R][b]	(N_{Ge}/N_{Pt})[c]
P	0	0	76	72	1.6	1.3	1.4	–	–
Ge1/12	1/12	230	62	63	1.5	1.6	1.6	[0.10, 2.52]	0.03
Ge1/8	1/8	350	65	65	1.3	1.5	1.5	[0.10, 2.54]	0.02
Ge1/2	1/2	1400	62	63	1.3	1.6	1.6	[0.15, 2.54]	0.03
Ge1	1	2800	34	57	1.4	3	1.8	[0.35, 2.46]	0.06
Ge2	2	5600	15	49	1.7	6.8	2.0	[0.40, 2.46]	0.08

[a] Calculated upon the number of accessible Pt using spherical particle model.
[b] N: is the coordination number of Ge; R is their mean distance, in Angstrom units.
[c] Atomic ratio.

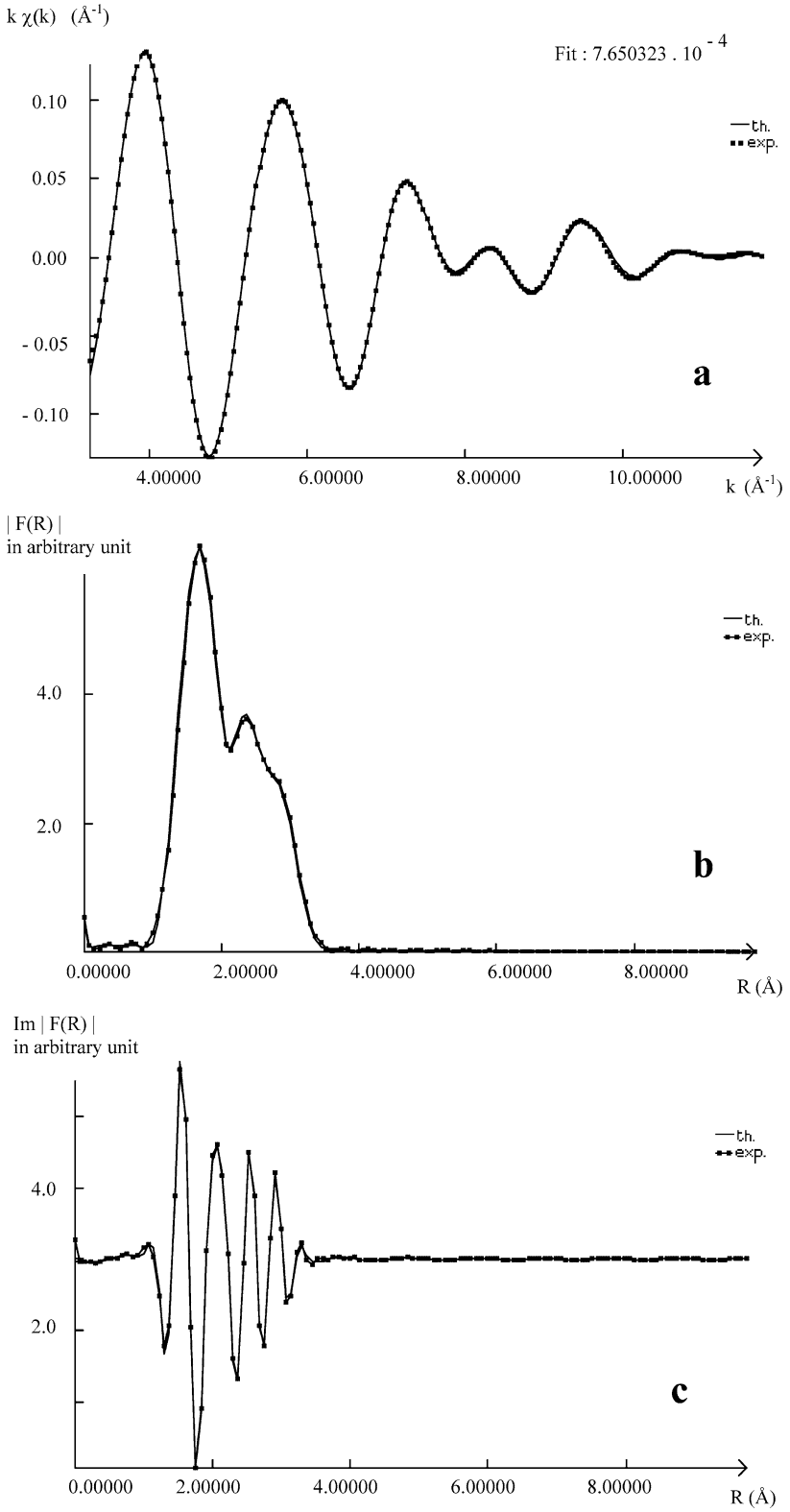

Fig. 1. Typical example of the agreement between experimental (exp) and fitted (th) data for **Ge1/2** sample. Reciprocal space (a), direct space: modulus (b) and imaginary (c) parts of the Fourier transformation are shown.

ples, more Ge was found in the neighborhood of Pt (N_{Pt}/N_{Ge} increased) and the Pt–Ge bond length was shortened. This indicates that Ge atoms (or small Ge ensembles) were intercalated in the Pt subsurface layers or in the particles, likely forming Pt_xGe_y solid solutions. Thus, a "bulk bimetallic system" was formed.

The low N_{Ge}/N_{Pt} ratio as opposed to that expected suggests that a part of Ge atoms may not interact with Pt. Germanium

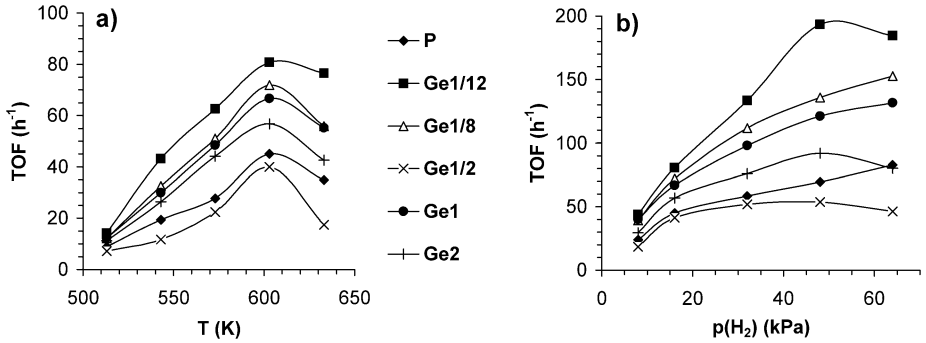

Fig. 2. Turnover frequencies (TOF) on different catalysts in hexane transformation as a function of temperature at $p(n\mathrm{H}):p(\mathrm{H_2}) = 1.3{:}16$ kPa (a) and hydrogen pressure at $T = 603$ K (b). TOF values were calculated upon accessible Pt atoms measured by CO-IR (Table 1) and length of the run $t = 5$ min as the "contact time."

Table 2
Turnover frequency (TOF) values (in h^{-1}) in hexane transformation calculated upon accessible Pt atoms measured by hydrogen adsorption (Table 1) in the same run shown in Fig. 2, $p(n\mathrm{H}) = 1.3$ kPa, $t = 5$ min

T (K)	513	543	573	603					633
$p(\mathrm{H_2})$ (kPa)	16	16	16	8	16	32	48	64	16
P	9	19	27	23	43	56	67	80	34
Ge1/12	14	44	64	45	82	136	197	188	78
Ge1/8	12	33	51	39	72	112	136	153	56
Ge1/2	8	13	25	20	46	58	60	52	20
Ge1	21	50	81	67	112	164	203	221	92
Ge2	37	86	144	96	185	248	300	262	139

was also present in the form of GeO_x that can even be located in the vicinity of Pt particles.

3.2. Reactions of hexane

The activity in hexane transformation was expressed as TOF values. The number of Pt_{surf} was calculated from the CO-IR data (Fig. 2). In general, the **Ge1/2** sample had the lowest activity, and **Ge1/8** and **Ge1/12** were most active in hexane transformation (Fig. 2). The **Ge1** and **Ge2** samples were slightly more active than the monometallic **P** sample. The dispersion values calculated from H_2 chemisorption indicate the surface fraction where hydrogen dissociation can occur. Because any reaction of hexane starts with C–H bond dissociation, it may not be an oversimplification to consider those sites as representing the active surface fraction. Table 2 shows that "bulk bimetallics" **Ge2** and **Ge1** also resulted in high TOF values when calculated from H_2 chemisorption, because the number of potentially active surface Pt atoms in the denominator was much smaller than those calculated from CO-IR and TEM measurements (Table 1). The activity of **Ge1/2** is apparently the lowest (Fig. 2; Table 2) because it contains the most Ge in the surface position (EXAFS results).

These results point to one possible weakness of the TOF calculation. TOF is rather sensitive to the method of determining the accessible active sites, usually estimated as the number of surface noble metal atoms from dispersion measurements. But one cannot be sure which inherent deficiencies of the applied method are inadvertently involved. For example, there may be sites that cannot adsorb hydrogen, but determining whether they are completely inactive is difficult. In the case of bulk bimetallic samples with high Ge loading, certain sites can adsorb CO while limiting hydrogen adsorption (Table 1). These special sites can or cannot adsorb hexane molecules, although if no neighboring hydrogen is present, then these adsorbed entities are likely inactive. The available experimental results are insufficient to provide a final answer to this problem.

The TOF curves exhibited maxima as a function of hydrogen pressure in the **Ge1/12**, **Ge1/2**, and **Ge2** samples (Fig. 2b). Only the positive hydrogen order branch [43] appeared in other cases; the maxima must be around 64 kPa (Fig. 2b). The maximum activity as a function of hydrogen pressure indicates the optimum hydrogen pressure at a given temperature [44,45]. This optimum is around 52–64 kPa at 603 K for monofunctional Pt catalysts [37], in good agreement with the results presented in Fig. 2b. These maxima shift to higher hydrogen pressure with increasing temperature [44]. As opposed to monometallic Pt catalysts [36,37,43,44], the negative hydrogen order range can be reached at high temperatures only with our Pt–Ge samples. This is clearly visible in Fig. 2a, because the activity values have a maximum at 603 K as a function of temperature when $p(n\mathrm{H}):p(\mathrm{H_2}) = \text{constant} = 1.3{:}16.0$ kPa. The rather parallel activity curves indicate that the optimum hydrogen pressure is similar for all samples; consequently, the differences between the samples should be due to the different structure of active sites rather than to the different effective surface hydrogen pressures [46].

Some representative selectivity data in hexane transformation are presented in Table 3. The C_6 saturated products (i.e., isomers + MCP + cyclohexane) were most abundant in all cases. Selectivity toward isomer formation increased as a function of hydrogen pressure, whereas that of MCP decreased proportionally, as observed earlier on Pt [37,43]. Compared with MCP and isomers, the selectivity of benzene and fragments showed smaller changes as a function of hydrogen pressure and temperature. Traces of hexenes appeared. **Ge2** was the only sample resulting in a noticeable amount (∼3%) of open-chain hexenes at low H_2 pressure and high temperature ($p(\mathrm{H_2}) = 8$ kPa; $T = 663$ K). This result is in agreement with the earlier observation that dehydrogenation can occur on small Pt islands or even on a single Pt atom [36,47]. The number and/or the activity of the presumed single Pt sites surrounded by Ge atoms can be large in this case.

Table 3
Selectivity (in %) of different product classes in hexane transformation at selected conditions on different samples; $p(n\mathrm{H})$= 1.3 kPa and $t = 5$ min in all cases. Corresponding activity data can be found in Fig. 2 and Table 2

	P			**Ge1/12**			**Ge1/8**			**Ge1/2**			**Ge1**			**Ge2**		
T (K)	543	603		543	603		543	603		543	603		543	603		543	603	
$p(\mathrm{H_2})$ (kPa)	16	16	64	16	16	64	16	16	64	16	16	64	16	16	64	16	16	64
$<C_6$	7	11	20	4	9	10	6	9	14	9	15	31	7	9	24	5	10	16
Isomers	43	40	60	44	26	64	30	26	64	45	29	50	48	31	55	52	32	61
Hexenes	0	0	0	0	1	0	0	0	0	0	0	0	0	1	0	0	1	0
MCP[a]	41	28	4	44	48	14	58	48	8	37	38	7	36	41	8	33	40	7
Benzene	9	21	16	8	16	12	0	17	1	9	18	11	9	18	13	9	18	17
Cyclohexane	0	0	0	0	0	0	6	0	13	0	0	1	0	0	0	0	0	0
C_6 satu/unsatu[b]	9.3	3.2	3.9	11.0	4.3	6.5	∞[c]	4.3	97.4	9.1	3.7	8.5	9.3	3.8	4.8	9.4	3.9	4.0

[a] Methylcyclopentane.
[b] Ratio of saturated and unsaturated C_6 products = (isomers + MCP + cyclohexane)/(hexenes + benzene).
[c] "∞" sign means result is infinite.

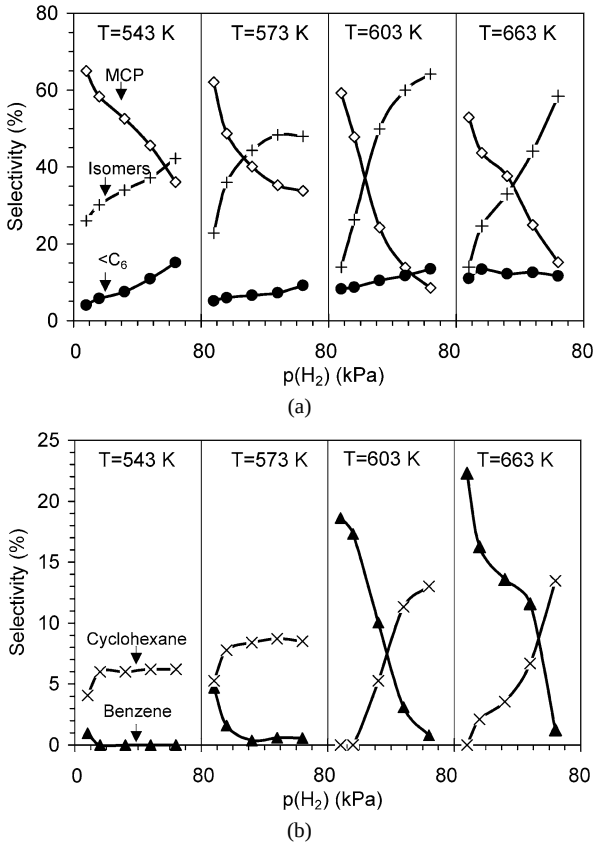

Fig. 3. Selectivity of different products formed from hexane on **Ge1/8** sample as a function of hydrogen pressure at different temperatures; $p(n\mathrm{H}) = 1.3$ kPa and $t = 5$ min.

The ratio of C_6 saturated and unsaturated products increased with hydrogen pressure and decreased with temperature (Table 3). It was highest in the **Ge1/8** sample and decreased, as a rule, with increasing Ge content above 1/8 monolayer.

Cyclohexane appeared in marked amounts only in the **Ge1/8** sample; trace amounts were found in **Ge1/2**. Cyclohexane usually is not produced from hexane on monofunctional Pt catalysts [37,39,40,43,44,48,49]. In this paper we extended the range of experimental parameters compared with our preliminary work [14] for elucidating the conditions of cyclohexane formation (Fig. 3). The amount of cyclohexane increased with $p(\mathrm{H_2})$ and decreased with increasing temperature (Table 3 and Fig. 3). The selectivity of benzene plus cyclohexane was nearly constant as a function of hydrogen pressure (Fig. 3). The value of that sum increased with increasing temperature. At low temperatures (543 and 573 K), hardly any benzene was formed (due in part to unfavorable thermodynamics). The selectivity of cyclohexane was constant as a function of $p(\mathrm{H_2})$ at $T \leqslant 573$ K and $p(\mathrm{H_2}) \geqslant 160$ kPa.

Table 4
Residual activity ($\mathrm{TOF/TOF_0}$) and selectivity (S/S_0) in standard test reaction ($p(n\mathrm{H})/p(\mathrm{H_2}) = 1.3/16$ kPa, $T = 603$ K) at $t = 5$ min and 50 min reaction time after intentional carbonization by hexane/hydrogen treatment. $\mathrm{TOF_0}$ and S_0 are well-reproducible results of test reaction on regenerated catalysts, while TOF and S were obtained on samples carbonized by $p(n\mathrm{H}):p(\mathrm{H_2}) = 1.3{:}8$ kPa at $T = 603$ K for 20 min

	P		**Ge1/12**		**Ge1/8**		**Ge1/2**		**Ge1**		**Ge2**	
t (min)	5	50	5	50	5	50	5	50	5	50	5	50
$\mathrm{TOF/TOF_0}$	0.5	0.7	0.3	0.8	0.1	0.8	0.1	0.8	0.4	0.8	0.6	0.8
S/S_0												
$<C_6$	1.1	1.0	2.2	1.8	2.4	1.4	1.9	1.4	1.2	1.1	1.2	1.1
Isomers	0.8	0.9	0.6	0.7	0.9	0.9	1.0	0.8	0.8	0.8	0.7	0.8
Hexenes	2.2	1.1	1.0	0.6	0.0	0.7	0.3	0.8	2.0	1.4	1.9	1.3
MCP	1.1	1.0	1.1	1.0	0.9	1.0	0.9	1.0	1.1	1.1	1.1	1.1
Benzene	0.9	1.1	1.1	1.2	1.1	1.1	1.1	1.2	1.0	1.1	1.0	1.1

Table 4 shows hexane transformation in the standard test reactions at 603 K with $p(n\mathrm{H}):p(\mathrm{H_2}) = 1.3{:}16$ kPa, following intentional carbonization by hexane/hydrogen treatment at $p(n\mathrm{H}):p(\mathrm{H_2}) = 1.3{:}8$ kPa at 603 K for 20 min. This method has been applied for the study of deactivation of different Pt black catalysts by carbonaceous deposits [39–42]. The Pt–Ge samples lost 40–90% of their regenerated activity on carbonizing treatment at the beginning of the test run, $t = 5$ min (Table 4), but much of this activity was recovered by the end of the test reaction, $t = 50$ min. Obviously, the presence of excess hydrogen in the test reaction mixture exerted this regeneration [39]. Comparing the ratios of the residual parameters (TOF and S) measured at the end of the test run ($t = 50$ min) with the analogous values on regenerated catalysts ($\mathrm{TOF_0}$ and S_0) demonstrates that the $\mathrm{TOF/TOF_0}$ and S/S_0 values were about the

same. **Ge1/12**, **Ge1/8**, **Ge1/2**, and **Ge1** displayed the lowest residual activity at 5 min of reaction time; of these, **Ge1/8** and **Ge1/2** had the lowest values (Table 4). The **Ge2** sample behaved very much like the monometallic **P** catalyst.

Similar to earlier observations on Pt black [39–41] and on supported Pt catalysts [42], it was the isomer selectivity that decreased most pronouncedly on deactivation (Table 4). The benzene and MCP selectivity remained about the same ($S/S_0 =$ 1.0–1.1). As a rule, the selectivity of fragments increased on deactivated catalysts, especially in those cases with stronger deactivation (Table 4). The opposite effect was found earlier with monometallic Pt catalysts [39–42], in which hexene selectivity increased dramatically under similar conditions.

3.3. Benzene and cyclohexene transformation

The only product of benzene transformation was cyclohexane. The results of this reaction presented in Fig. 4. The TOF increased continuously with $p(H_2)$ and decreased with temperature (Fig. 4). The order of the activity was **Ge1/8** < **Ge1/2** ≪ **Ge1/12** < **P** < **Ge1** < **Ge2**, calculated using the dispersion values from CO-IR measurement. The TOF values for **Ge1** and **Ge2** would even be higher if we applied the accessible Pt atoms calculated from hydrogen adsorption. The extremely low conversion on **Ge1/8** catalyst reported earlier [14] was thus confirmed by the present extended study. The possible selective deposition of Ge on the **Ge1/8** sample, blocking high-coordination sites (100 and 111), is considered in detail in Section 4.

Cyclohexene formed two products: cyclohexane and benzene. The reactions include hydrogenation and dehydrogenation or "disproportionation": $3C_6H_{10} \leftrightarrow C_6H_6 + 2C_6H_{12}$ ("irreversible catalysis" [50]). Cyclohexene gave mostly benzene on Pt with short contact times (in a pulse system). Recirculating it for several minutes even in He, the ratio of cyclohexane to benzene was 2:1, corresponding to the foregoing equation [51]. Thus, the disproportionation of cyclohexene occurs through disproportionation of surface hydrogen between benzene and cyclohexane with an active participation of hydrogen given off during primary benzene formation and "retained" by Pt.

The activities in cyclohexene reaction are presented in Fig. 5. The TOF values were almost constant as a function of hydrogen pressure between 8 and 64 kPa at 453 K (Fig. 5b). It increased slightly as a function of temperature at $p(H_2) = 16$ kPa (Fig. 5a). The activity order in TOF values calculated using the Pt_{surf} values from CO-IR measurements was almost the opposite of that in benzene transformation (cf. Figs. 4 and 5): **P** < **Ge2** < **Ge1** < **Ge1/12** < **Ge1/2** < **Ge1/8**. **Ge1** and **Ge2** were the most active when TOF values were calculated from H_2 chemisorption data.

The ratio of benzene to cyclohexane formed from cyclohexene in excess hydrogen was compared with the thermodynamic equilibrium of these two molecules, because cyclohexene is rather reactive under these conditions [49,52]. We reached almost total conversion in 5 min. Fig. 6 presents the ratios of cyclohexane to benzene formed from cyclohexene in comparison with their thermodynamically calculated ratios (considering the equilibrium reaction $C_6H_6 + 3H_2 \leftrightarrow C_6H_{12}$). Clearly, the

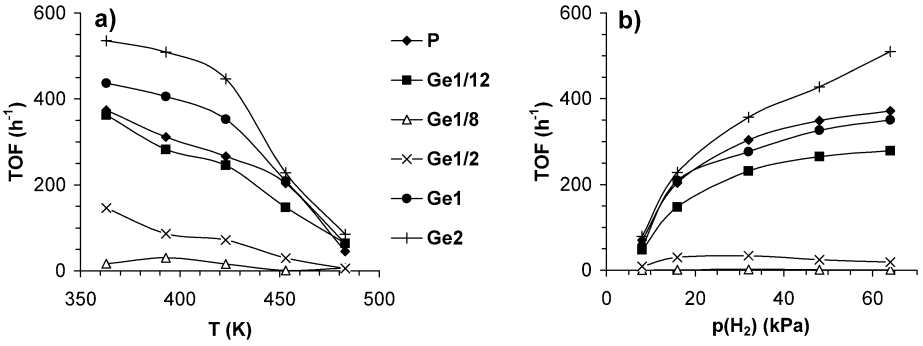

Fig. 4. Turnover frequencies (TOF) on different catalysts in benzene transformation as a function of temperature at $p(nH):p(H_2) = 1.3:16$ kPa (a) and hydrogen pressure at $T = 453$ K (b). TOF values were calculated upon accessible Pt atoms measured by CO-IR (Table 1) and length of the run $t = 5$ min as the "contact time."

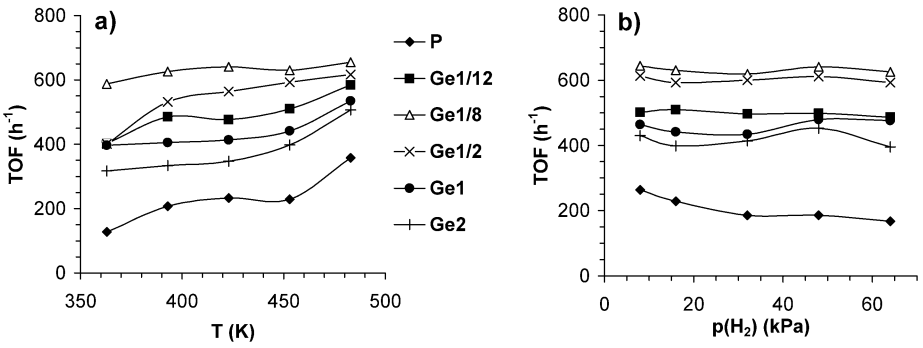

Fig. 5. Turnover frequencies (TOF) on different catalysts in cyclohexene transformation as a function of temperature at $p(nH):p(H_2) = 1.3:16$ kPa (a) and hydrogen pressure at $T = 453$ K (b). TOF values were calculated upon accessible Pt atoms measured by CO-IR (Table 1) and length of the run $t = 5$ min as the "contact time."

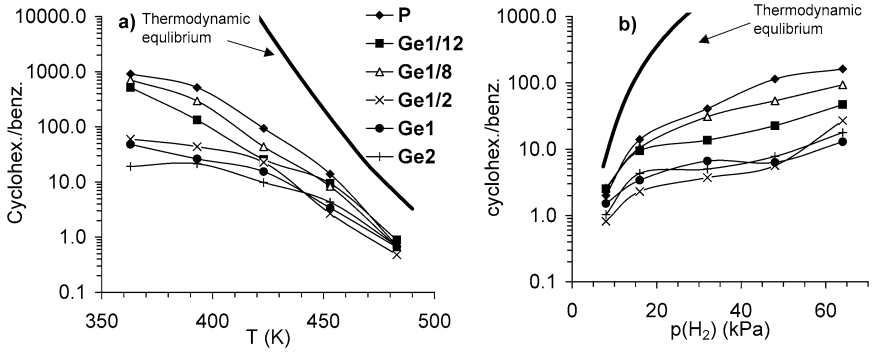

Fig. 6. Ratio of cyclohexane and benzene formed from cyclohexene on different catalysts as a function of temperature at $p(n\mathrm{H}):p(\mathrm{H_2}) = 1.3{:}16$ kPa (a) and hydrogen pressure at $T = 453$ K (b). Bold solid line represents the calculated thermodynamic equilibrium between benzene and cyclohexane (see text).

Table 5
The calculated free enthalpy change (Gibbs energy) and equilibrium constant of benzene hydrogenation at different temperatures

Temperature (K)	ΔG (kJ/mol)	K
300	−98	1.16E+17
350	−80	8.71E+11
400	−62	1.25E+08
450	−44	1.28E+05
500	−26	5.20E+02
550	−8	5.75E+00
600	10	1.35E−01
650	28	5.62E−03
700	46	3.69E−04

amount of benzene increased with increasing temperature and decreased with increasing hydrogen pressure. The cyclohexene/benzene ratio increased in the order **Ge2** $\lessapprox$ **Ge1** $\lessapprox$ **Ge1/2** < **Ge1/12** < **Ge1/8** < **P** < thermodynamic equilibrium (Fig. 6).

Table 5 presents the calculated Gibbs energy values and the equilibrium constants as a function of temperature for the benzene ↔ cyclohexane equilibrium. The enthalphy and entropy values were taken from a previous report [53]. The results clearly show that it is not possible to saturate benzene to cyclohexane above 600 K. The equilibrium is shifted toward cyclohexane at low temperature [52]. The increased hydrogen excess also shifts the equilibrium to cyclohexane, as shown in Table 6. The thermodynamically calculated equilibrium ratio cannot be reached in all cases. The thermodynamic parameters show the equilibrium in spontaneous reaction, under infinite time; however, the difference between the calculated and the measured data points to a kinetic hindrance, that is, the efficiency of the catalyst in decreasing the activation energy of the different reactions. The measured data of cyclohexene transformation show lower amounts of cyclohexane than were predicted by the thermodynamic calculation. Thus cyclohexene produced benzene relatively more easily than cyclohexane [54]. This indicates that the activation energy of cyclohexene-to-cyclohexane transformation is higher than that of cyclohexene-to-benzene transformation. Consequently, the dehydrogenation of the first bond may be rate-limiting in consecutive dehydrogenation of cyclohexane to benzene. The results obtained in cyclohexene transformation were closest to the calculated equilibrium at high temperature and low hydrogen pressure (Fig. 6).

Table 6
The cyclohexane-to-benzene ratio at different temperatures and hydrogen pressures, if the starting mixture consists of 1.3 kPa benzene and "$p^0(\mathrm{H_2})$" kPa hydrogen

Temperature (K)	Cyclohexane/benzene				
$p^0(\mathrm{H_2})$ (kPa)	8	16	32	48	64
300	7.13E+12	1.92E+14	2.44E+15	9.48E+15	2.41E+16
350	5.35E+07	1.45E+09	1.84E+10	7.13E+10	1.81E+11
400	7.68E+03	2.07E+05	2.64E+06	1.02E+07	2.59E+07
450	1.25E+01	2.13E+02	2.70E+03	1.05E+04	2.66E+04
500	1.97E−01	1.37E+00	1.18E+01	4.26E+01	1.08E+02
550	2.83E−03	2.26E−02	1.70E−01	5.62E−01	1.32E+00
600	6.63E−05	5.30E−04	4.24E−03	1.43E−02	3.39E−02
650	2.77E−06	2.21E−05	1.77E−04	5.97E−04	1.42E−03
700	1.82E−07	1.45E−06	1.16E−05	3.92E−05	9.30E−05

4. Discussion

The reactions of hexane transformation [20,43] are summarized in Scheme 1. The first step can be the dissociation of the first C–H bond of the saturated hydrocarbon reactant [20,48,55–57]; this may even be the rate-determining step under hydrogen-rich conditions [58]. A "reactive adsorption" (i.e., C_6H_{14} + Pt–H–Pt to Pt–C_6H_{13} + Pt–H) was also suggested as an alternative pathway [59]. This can be the surface intermediate that can cyclize (on two-atom Pt sites) to give an adsorbed C_5-cyclic species, which can desorb as MCP or can give skeletal isomers (Scheme 1) [20,48,56,57]. Their ratio is governed by the available surface hydrogen [46,55,60,61], resulting in a mirror image of MCP and isomer selectivity as a function of hydrogen pressure (Fig. 3).

Benzene is reported to form by "stepwise aromatization" from hexane on monofunctional Pt catalysts [48,62–64]. This reaction involves open-chain hexadiene and triene intermediates, with cyclization then occurring by ring closure of a *cis–cis* hexadiene or *cis–cis*-hexatriene on these sites to give cyclohexadiene (Scheme 1). This latter reaction reportedly requires ensembles of three Pt atoms in triangular symmetry [30]. This route has been confirmed by the appearance of cyclohexadiene from both *trans*- and *cis*-hexa-1,3,5-triene reactants on Pt [62]. The *trans* ↔ *cis* isomerization of such unsaturated surface compounds also requires hydrogen but can still occur with less

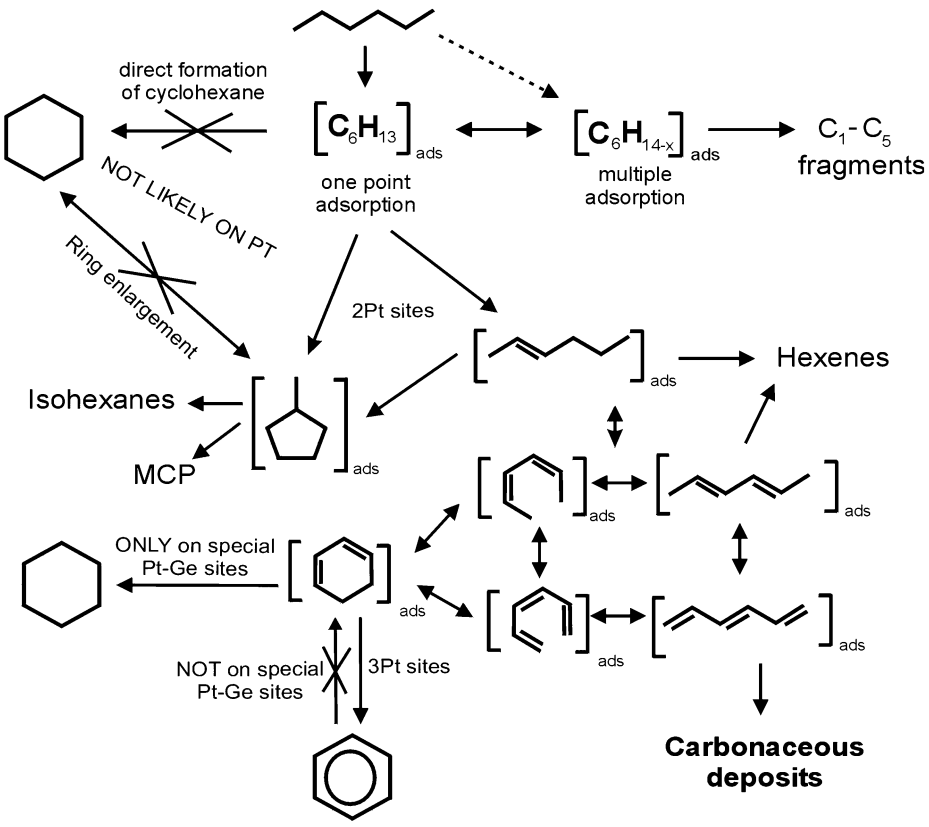

Scheme 1. A suggested reaction mechanism of hexane transformation on Pt catalysts, a synthesis of earlier published propositions [43,48,52,62].

H(ads) present. As opposed to the *cis*-trienes, the *trans*-isomers can polymerize to carbonaceous deposits when insufficient hydrogen is present [43,48,62] (Scheme 1). The last step may be "hydrogenative desorption" of surface C_6H_{6-x} benzene precursors, that is, an unsaturated C_6-cyclic compound (Scheme 1).

During the stepwise aromatization, unsaturated intermediates can also desorb and appear in the gas phase in the absence of sufficient hydrogen (Scheme 1); in most cases these are hexenes, but hexadienes have also been detected when hexane was reacted over supported bimetallic catalysts, such as PtSn or PtPb [65]. Hexenes are exclusive primary product with low hydrogen excess, but they do not appear in the gas phase with much hydrogen present [66] (Scheme 1).

Cyclohexane cannot be observed among the products of hexane transformation on most monofunctional Pt catalysts. The usual assumption for cyclohexane formation is acid-catalyzed ring enlargement of the primary C_5-cyclic intermediate from hexane [27]. This route is not likely on monofunctional Pt, as shown in Scheme 1. In our study, cyclohexane appeared among the products on the **Ge1/8** sample (Table 3, Fig. 3). Cyclohexane can be formed from the primary intermediate of the ring closure step (an unsaturated C_6-cyclic compound, such as cyclohexadiene [67]) by its hydrogenation when the abundance of three-atom sites [20,48] is too small and the hydrogen excess is high. This was also deduced from radiotracer experiments, reacting hexane–[^{14}C]-cyclohexane mixtures on Pt-KL [68]. On the other hand, when the abundance of three-atom sites is sufficiently high, usually on monometallic Pt catalysts, this cyclic intermediate preferably or exclusively desorbs as benzene. Cyclohexane selectivity as a function of hydrogen pressure was a mirror image with benzene selectivity (Fig. 3), so it seems very reasonable to relate these two reactions to one another (Scheme 1). Thus the appearance of cyclohexane from hexane on certain Pt–Ge catalysts (on **Ge1/8** and in traces in **Ge1/2**; see Table 3) can be due to the Ge deposition on Pt, selectively blocking three-atom ensembles (Scheme 1).

Fragmentation must have a separate reaction route from the key intermediate (Scheme 1), requiring ensembles of several Pt atoms [69,70]. Earlier observations on monofunctional Pt catalysts [37,43] showed that this reaction lies on a different compensation line than others. Several authors have attributed deeply dissociated (e.g., α, α, γ) intermediate(s) to hydrogenolysis [69,70], the formation and decomposition of which must involve several elementary steps. Internal rupture has also been reported and considered closely related to isomerization, and may involve a not too deeply dehydrogenated intermediate [47, 71]. Here the geometric requirements are not as strict as in aromatization. It is possible that the number of triangular three-atom ensembles for aromatization is small on **Ge1/8** [30,48], but the two-atom ensembles needed for C_5-cyclization and ring opening [72] and multiple Pt atom sites in "random" arrangement for fragmentation [70] are present.

The sum of selectivities of isomers plus MCP is 57–88% (Table 3), highest on the "surface bimetallics" with low levels of germanium, **Ge1/12** and **Ge1/8** (72–88%). The summarized selectivities of the two reactions requiring larger ensembles (hydrogenolysis and aromatization) are always lower, and are lowest with the two samples mentioned. **Ge1/2** with lowest overall

activity (Table 2) and the two "bulk bimetallics": **Ge1** and **Ge2** showed somewhat higher activity in these two reactions (30–40% vs. 12–25%). This indicates the existence of ensembles of three to four Pt atoms on catalysts with much surface Ge or Ge in their bulk—even if these represent isolated islands.

The other two reactions, hydrogenation of benzene and cyclohexene, also provide information on catalytic sites that can activate reactions involving C–H bonds. Benzene hydrogenation can start with the adsorption of the aromatic ring parallel to the catalyst surface on three Pt atoms with (111) symmetry. The "sextet model" of Balandin [50,73] assumed the addition of six H atoms apparently in a single step. Radiotracer studies [74] have shown that in fact a triangular reaction occurs on different metals; "direct" hydrogenation to cyclohexane (the main reaction at low conversions) was accompanied by a stepwise reaction involving cyclohexene as an intermediate. This latter route may involve parallel π-adsorption as an initial step, followed by the formation of intermediate(s) adsorbed "edgewise" [75]. A π-allyl intermediate (i.e., the interaction of 3 C atoms with the catalyst surface) was also suggested [76]. The transformation of cyclohexene was explained by both sextet and doublet mechanisms [50,77], involving "flat-lying" and "edgewise" chemisorption, respectively. But recent single crystal studies [78] on Pt(111) showed that the situation is more complex. Depending on the temperature, cyclohexene is adsorbed in a "half-chair" configuration on two metal atoms (at 130 K) "edgewise" by di-σ bonds at 220 K, but at temperatures practicable for hydrogenation (260–283 K) a "tilted" cyclo-C_6H_9 species is attached to 3 Pt atoms, possibly in a way analogous to a π-allyl intermediate. The sites for these intermediates are different from those required for dehydrogenation to benzene (300–383 K), which occurs via a "flat-lying" intermediate.

Ge1/8 was almost inactive in benzene hydrogenation but was very active in cyclohexene transformation to cyclohexane (cf. Figs. 4 and 5). Thus, on the **Ge1/8** catalyst there was a low probability to form the "flat-lying" intermediate. Consequently, the high coordination sites of (111) symmetry must be selectively blocked by Ge. At the same time, the "edgewise" or "tilted" adsorption of cyclohexene was not hindered.

We now return to the interpretation of hexane transformation on the **Ge1/8** sample. Scheme 2 compares the possible conformation of the intermediate(s) in *cis–trans* isomerization of conjugated hexadienes on the Pt(111) surface. The partly dehydrogenated intermediates rotate freely and "stand up" on the surface. This structure is in fact very similar to that reported in an SFG study on Pt(111) single crystals in cyclohexene transformation [78]. In the case of monometallic Pt surface, this intermediate quickly lies down, and the unsaturated C_6-cyclic intermediate rapidly transforms to benzene (Scheme 2a). On the other hand, when other atoms are present (in our case, Ge), this intermediate cannot lie down and will be hydrogenated to cyclohexane (Scheme 2b).

The selective deposition of Ge can also be deduced from the catalytic results on intentionally carbonized samples (Table 4). Two major observations can be described:

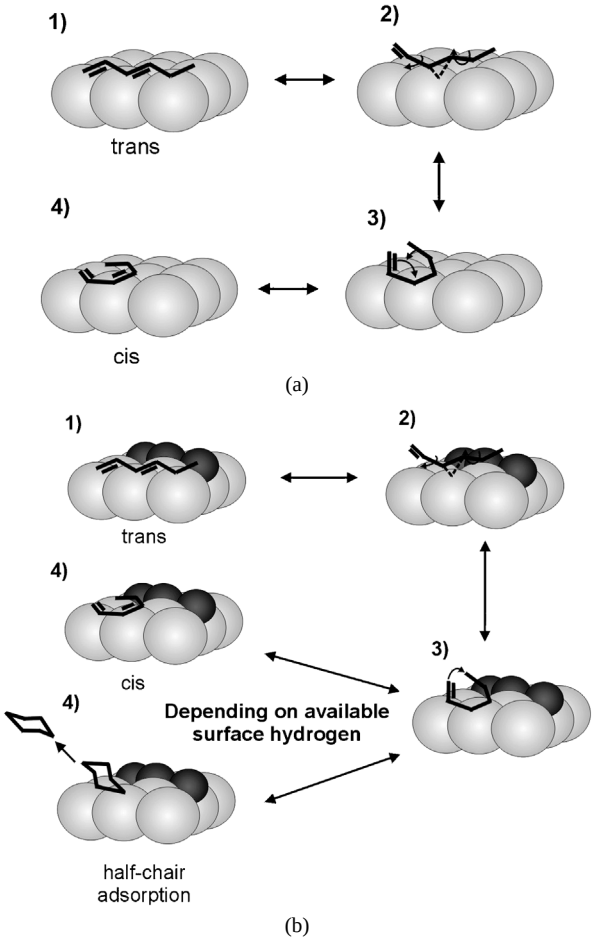

Scheme 2. *Trans–cis* isomerization of 1,3-hexadiene on Pt(100) surface (a) and on Pt surface partly occupied by Ge atoms (darker circles) (b).

(i) Pt–Ge catalysts with small, surface Ge loading (**Ge1/12**, **Ge1/8**, **Ge1/2**) showed low (0.1–0.3) residual activity at the beginning of the test run ($t = 5$ min) on intentionally carbonized samples. It increased up to 0.8 at the end of the test run ($t = 50$ min). On the other hand, catalysts with much Ge (**Ge1**, **Ge2**) as well as the Ge-free **P** sample lost only about half of their initial activity, and it increased up to 0.8 at the end of the test run.

(ii) Pt–Ge catalysts with small Ge loading showed *higher* fragmentation selectivities as opposed to the higher hexene formation on Pt without Ge and on catalysts with much Ge (Table 4).

Two different coke formation routes were postulated: the C_1 route and the polyene route [79]. Inert metals—such as Sn [30,47,80,81] or just Ge [14]—divide the contiguous Pt surface into smaller ensembles, and this hinders polymerization of unsaturated intermediates. Thus carbonization on Pt–Ge catalysts should take place mainly via the C_1-route; that is, carbon precursors are fragmented and dehydrogenated forming C, CH, or CH_2, species on the surface [79,82]. Formation of C–C bonds between surface CH_x species can occur even at low temperature [83]. The C_1 route could even be more favorable when high-coordination sites are selectively blocked by Ge ("sur-

face bimetallics"). In this case, residual C_1 species occupy low-coordination sites after intentional carbonization (high-coordination sites are already blocked by Ge), consequently the residual activity is low at the beginning of the subsequent test reaction (Table 4). On the other hand, the excess hydrogen in the test run can remove these C_1 species [84,85]. It leads to the appearance of many fragments in the gas phase, as well as the recovery of initial activity.

In addition to the geometric interpretation other effects may play important role. The coexistence of electronic and geometric effects was demonstrated on supported Pt–Sn catalysts [86]. The electron acceptor effect of Ge also may be important [35,87]. The "virtual" hydrogen concentration on the clean, carbon-free, Pt sites of **Ge1/8** can be higher than that corresponding to the gas phase [46,88]. This abundant hydrogen may cause favored formation of C_6-saturated products (isomers, MCP, and cyclohexane) as opposed to aromatization [46,47].

5. Conclusion

In this study, adding germanium to a monofunctional Pt/Al_2O_3 catalyst by controlled surface reaction of organometallic Ge precursor, Ge(n-C_4H_9)$_4$, resulted in special Pt–Ge interactions. Deposition of smaller amounts of Ge led to surface bimetallic catalysts. Ge in amounts of $1/12$ monolayer resulted in randomly scattered Ge atoms on the surface of Pt, as confirmed by EXAFS measurement and catalytic studies. Ge was selectively deposited on high-coordination sites, but because of its low amount, it hardly affected the catalytic behavior compared with the Ge-free parent catalyst. A $1/8$ monolayer of Ge was still located on Pt as single atoms (EXAFS), but the selective poisoning of high-coordination sites by Ge can be clearly deduced from catalytic observations in this case. Deposition of $1/2$ monolayer of Ge resulted in less selective deposition than in the deposition of $1/8$ monolayer. This catalyst showed the lowest TOF values in hexane conversion, because of the large amount of Ge on the surface. The selective deposition was deduced from the following observations:

(i) The **Ge1/8** sample was almost inactive in benzene hydrogenation but was very active in cyclohexene transformation.
(ii) This sample transformed hexane with high selectivity into saturated C_6 products and formed hardly any benzene. The formation of cyclohexane from hexane was also observed here (and in the case of **Ge1/2** in traces).
(iii) The C_1 carbonization route occurred mainly on low-coordination sites, because the high-coordination sites were selectively blocked by Ge. A pronounced activity loss was seen on intentionally carbonized samples at the beginning of the test run (which could be recovered by the end of the test run), concomitant with the appearance of much fragments.

Adding one to two monolayers of Ge caused a new type of interaction between Pt and Ge. EXAFS results revealed a shorter Pt–Ge distance and more Ge in the vicinity of Pt atoms. A solid solution of Pt–Ge (i.e., a bulk bimetallic system) containing sites that adsorb CO but do not adsorb hydrogen may have arisen here. However, Pt atoms not interacting with Ge showed similar activity and selectivity in hydrocarbon transformation as the original parent catalyst.

Acknowledgments

This project was supported in part by the Hungarian National Science Foundation (grant OTKA T037241) and the MTA-CNRS cooperation framework program (no. 17182). A.W. was the recipient of a Bolyai Grant from the Hungarian Academy of Sciences.

References

[1] V. Ponec, G.C. Bond, Catalysis by Metals and Alloys, Stud. Surf. Sci. Catal., vol. 95, Elsevier, Amsterdam, 1995, pp. 227–228.
[2] J. Barbier, in: G. Ertl, H. Knözinger, J. Weitkamp (Eds.), Handbook of Heterogeneous Catalysis, vol. 1, Verlag Chemie, Weinheim, 1997, pp. 257–264.
[3] S. Göbölös, J.L. Margitfalvi, in: J.J. Spivey (Ed.), Catalysis. Specialist Periodical Report, vol. 17, The Royal Society of Chemistry, London, 2004, p. 1.
[4] J.P. Candy, B. Didillon, E.L. Smith, T.B. Shay, J.M. Basset, J. Mol. Catal. 86 (1984) 179.
[5] R. Mélendrez, G. Del Angel, V. Bertin, M.A. Valenzuela, J. Barbier, J. Mol. Catal. A 157 (2000) 143.
[6] C. Micheaud-Especel, D. Bazin, M. Guérin, P. Marécot, J. Barbier, React. Kinet. Catal. Lett. 69 (2000) 209.
[7] S. Szabó, Int. Rev. Phys. Chem. 10 (1991) 207.
[8] J.L. Margitfalvi, S. Szabó, F. Nagy, Stud. Surf. Sci. Catal. 17 (1986) 373.
[9] B. Coq, F. Figuéras, Coord. Chem. Rev. 178–180 (1998) 1753.
[10] O.A. Ferretti, J.P. Bournonville, G. Mabilon, G. Martino, J.P. Candy, J.M. Basset, J. Mol. Catal. 67 (1991) 283.
[11] J.L. Margitfalvi, I. Borbáth, A. Tompos, Preparation of Catalysts VII, Stud. Surf. Sci. Catal., vol. 118, Elsevier, Amsterdam, 1998, pp. 195–204.
[12] L. Pirault-Roy, D. Teschner, Z. Paál, M. Guérin, Appl. Catal. A 245 (2003) 15.
[13] D. Teschner, L. Pirault-Roy, D. Naud, M. Guérin, Z. Paál, Appl. Catal. A 252 (2003) 421.
[14] A. Wootsch, L. Pirault-Roy, J. Leverd, M. Guérin, Z. Paál, J. Catal. 208 (2002) 490.
[15] B. Didillon, A. El Mansour, J.P. Candy, J.P. Bournonville, J.M. Basset, Heterogeneous Catalysis and Fine Chemicals II, Stud. Surf. Sci. Catal., vol. 59, Elsevier, Amsterdam, 1991, p. 137.
[16] J.L. Margitfalvi, S. Göbölös, M. Hegedüs, E. Tálas, Heterogeneous Catalysis and Fine Chemicals I, Stud. Surf. Sci. Catal., vol. 41, Elsevier, Amsterdam, 1988, p. 145.
[17] B. Coq, A. Bittar, F. Figueras, Appl. Catal. 59 (1990) 103.
[18] B. Coq, A. Chaqroune, F. Figueras, B. Nciri, Appl. Catal. A 82 (1992) 231.
[19] J.H. Sinfelt, in: G. Ertl, H. Knözinger, J. Weitkamp (Eds.), Handbook of Heterogeneous Catalysis, vol. 14, Verlag Chemie, Weinheim, 1997, p. 1939.
[20] Z. Paál, in: G.J. Antos, A.M. Aitani (Eds.), Catalytic Naphtha Reforming, second ed., Dekker, New York, 2004, p. 35.
[21] D.L. Trimm, in: G. Ertl, H. Knözinger, J. Weitkamp (Eds.), Handbook of Heterogeneous Catalysis, vol. 3, Verlag Chemie, Weinheim, 1997, p. 1263.
[22] J. Barbier, Appl. Catal. 23 (1986) 225.
[23] G.C. Bond, Appl. Catal. 149 (1997) 3.

[24] J.P. Boitiaux, J.M. Devès, B. Didillon, C.R. Marcilly, in: G.J. Antos, A.M. Aitani, J.M. Parera (Eds.), Catalytic Naphtha Reforming, Dekker, New York, 1995, p. 79.
[25] J.A. Rabo, in: L. Guczi, F. Solymosi, P. Tétényi (Eds.), Proceedings of the 10th ICC, Akadémiai Kiadó, Budapest, 1992, p. 1.
[26] S. Sivasanker, P. Ratnasamy, in: G.J. Antos, A.M. Aitani, J.M. Parera (Eds.), Catalytic Naphtha Reforming, Dekker, New York, 1995, p. 483.
[27] G.J. Antos, A.M. Aitani (Eds.), Catalytic Naphtha Reforming: Science and Technology, second ed., Dekker, New York, 2004.
[28] G. Martino, P. Courty, C. Marcilly, in: G. Ertl, H. Knözinger, J. Weitkamp (Eds.), Handbook of Heterogeneous Catalysis, vol. 4, Verlag Chemie, Weinheim, 1997, p. 1801.
[29] R.T.K. Baker, K. Laubernds, A. Wootsch, Z. Paál, J. Catal. 193 (2000) 165.
[30] P. Biloen, J.N. Helle, H. Verbeek, F.M. Dautzenberg, W.M.H. Sachtler, J. Catal. 63 (1980) 112.
[31] J.L. Margitfalvi, I. Borbáth, E. Tfirst, A. Tompos, Catal. Today 43 (1998) 29.
[32] P.J. Lévy, V. Pitchon, V. Perrichon, M. Primet, M. Chevrier, C. Gauthier, J. Catal. 178 (1998) 363.
[33] L. Pirault-Roy, M. Guérin, F. Maire, P. Marécot, J. Barbier Appl. Catal. A 199 (2000) 109.
[34] A. Michalowicz, EXAFS pour le MAC, Logiciels pour la chimie, vol. 102, Société Française de Chimie, Paris, 1991, p. 1.
[35] A. Borgna, T.F. Garetto, C.R. Apesteguia, B. Moraweck, Appl. Catal. A 182 (1999) 189.
[36] Z. Paál, H. Groeneweg, J. Paál-Lukács, J. Chem. Soc., Faraday Trans. 86 (1990) 3159.
[37] A. Wootsch, Z. Paál, J. Catal. 185 (1999) 192.
[38] M. Boudart, in: G. Ertl, H. Knözinger, J. Weitkamp (Eds.), Handbook of Heterogeneous Catalysis, vol. 3, Verlag Chemie, Weinheim, 1997, p. 958.
[39] Z. Paál, A. Wootsch, K. Matusek, U. Wild, R. Schlögl, Catal. Today 65 (2001) 13.
[40] N.M. Rodriguez, P.E. Anderson, A. Wootsch, U. Wild, R. Schlögl, Z. Paál, J. Catal. 197 (2001) 365.
[41] Z. Paál, U. Wild, A. Wootsch, J. Find, R. Schlögl, Phys. Chem. Chem. Phys. 3 (2001) 2148.
[42] Z. Paál, A. Wootsch, R. Schlögl, U. Wild, Appl. Catal. A 282 (2005) 135.
[43] A. Wootsch, Z. Paál, J. Catal. 205 (2002) 86.
[44] Z. Paál, in: Z. Paál, P.G. Menon (Eds.), Hydrogen Effects in Catalysis, Dekker, 1988, p. 449.
[45] G.C. Bond, L. Hui, J. Catal. 137 (1992) 462.
[46] (a) Z. Paál, G. Székely, P. Tétényi, J. Catal. 58 (1979) 108;
(b) G.C. Bond, R.H. Cunningham, J. Catal. 166 (1997) 172.
[47] V. Ponec, Adv. Catal. 32 (1983) 149.
[48] Z. Paál, Adv. Catal. 29 (1980) 273.
[49] G.A. Somorjai, Chemistry in Two Dimensions: Surfaces, Cornell University Press, Ithaca, 1981.
[50] A.A. Balandin, Adv. Catal. 19 (1969) 1.
[51] Yu.I. Derbentsev, Z. Paál, Acta Chim. Hung. 73 (1972) 235.
[52] P. Tétényi, K. Schächter, Acta Chim. Acad. Sci. Hung. 50 (1966) 129.
[53] Handbook of Chemistry and Physics, eightieth ed., CRC Press, London, 1999.
[54] P. Tétényi, L. Babernics, K. Schächter, Acta Chim. Acad. Sci. Hung. 58 (1968) 321.
[55] Z. Paál, X.L. Xu, J. Paál-Lukács, W. Vogel, M. Muhler, R. Schlögl, J. Catal. 152 (1995) 252.
[56] G. Maire, G. Plouidy, J.C. Prudhomme, F.G. Gault, J. Catal. 4 (1965) 556.
[57] Y. Barron, G. Maire, M. Muller, F.G. Gault, J. Catal. 5 (1966) 428.
[58] P. Tétényi, Acta Chim. Acad. Sci. Hung. 40 (1964) 157.
[59] P. Parayre, V. Amir-Ebrahimi, F.G. Gault, A. Frennet, J. Chem. Soc., Faraday Trans. 76 (1980) 1704.
[60] M.G. Falco, S.A. Canavese, R.A. Comelli, N.S. Fígoli, Stud. Surf. Sci. Catal. 130 (2000) 2393.
[61] Z. Paál, J. Catal. 156 (1995) 301.
[62] Z. Paál, P. Tétényi, J. Catal. 30 (1973) 350.
[63] A.V. Teplyakov, B.E. Bent, J. Phys. Chem. B 101 (1997) 9052.
[64] B.H. Davis, Catal. Today 53 (1999) 443.
[65] Z. Paál, M. Dobrovolszky, J. Völter, G. Lietz, Appl. Catal. 14 (1985) 33.
[66] Z. Paál, X.L. Xu, Appl. Catal. 43 (1988) L1.
[67] H. Zimmer, V.V. Rozanov, A.V. Sklyarov, Z. Paál, Appl. Catal. 2 (1982) 51.
[68] L. Manninger, Z. Zhan, X.L. Xu, Z. Paál, Appl. Catal. 51 (1989) L7.
[69] J.R. Anderson, Adv. Catal. 23 (1973) 1.
[70] J.H. Sinfelt, Adv. Catal. 23 (1973) 91.
[71] F.G. Gault, Adv. Catal. 30 (1981) 1.
[72] Z. Paál, P. Tétényi, Nature 267 (1977) 234.
[73] A.A. Balandin, Z. Phys. Chem. B 2 (1929) 289.
[74] Yu.I. Derbentsev, Z. Paál, P. Tétényi, Z. Phys. Chem. (Frankfurt) 80 (1972) 51.
[75] J.L. Garnett, W.A. Sollich, J. Catal. 2 (1963) 350.
[76] J.J. Rooney, G. Webb, J. Catal. 3 (1964) 488.
[77] A.A. Balandin, I.I. Brusov, Z. Phys. Chem. B 34 (1936) 96.
[78] G.A. Somorjai, G. Rupprechter, J. Phys. Chem. B 103 (1999) 1623.
[79] A. Sárkány, H. Lieske, T. Szilágyi, L. Tóth, Proceedings of the 8th International Congress on Catalysis, vol. 2, Berlin, 1984, p. 613.
[80] B.H. Davis, G.A. Westfall, J. Watkins, J. Pezzanite, J. Catal. 42 (1976) 247.
[81] Z. Paál, A. Győry, I. Uszkurat, S. Olivier, M. Guérin, C. Kappenstein, J. Catal. 168 (1997) 164.
[82] G.C. Bond, Appl. Catal. A 149 (1997) 3.
[83] D.H. Fairbrother, X.D. Peng, M. Trenary, P.C. Stair, Surf. Sci. 285 (1993) L455.
[84] K. Matusek, A. Wootsch, H. Zimmer, Z. Paál, Appl. Catal. A 191 (2000) 141.
[85] A. Wootsch, C. Descorme, Z. Paál, D. Duprez, J. Catal. 208 (2002) 273.
[86] A. Palazov, C. Bonev, D. Shopov, G. Lietz, A. Sárkány, J. Völter, J. Catal. 103 (1987) 249.
[87] T.F. Garetto, A. Borgna, C.R. Apesteguia, Stud. Surf. Sci. Catal. 88 (1994) 369.
[88] J.A. Biscardi, E. Iglesia, J. Catal. 182 (1999) 117.